Influence of Sm-substitution on the crystal and electronic structure of the $FeBO_3$ oxide

OSMAN MURAT OZKENDIR[a,b*], ABDULCELİL YUZER[b]
[a]*Mersin University, Faculty of Technology, Energy Systems Engineering, 33400, Tarsus, Turkey*
[b]*Mersin University, Institute of Natural Science, Dept. of Nanotechnology and Advanced Materials, 33343, Mersin, Turkey*

Influences of Samarium substitution in the Ferric Borate oxide materials were investigated on their crystal, electric and electronic properties. Studies were mainly carried on the change in the crystal structure with the increasing Sm substitutions with the collected data from the synchrotron facilities. All prepared samples were determined as semiconductors with weak antiferromagnetic (AFM) ordering at the room temperatures. The main technique for the investigations was the X-ray absorption near-edge spectroscopy (XANES) and the collected data were used to probe in the electronic structure properties of the samples. Prominent changes and phase transitions in the crystal structure were observed according to the increasing Sm substitutions. Besides, iron atoms and their 3*d* levels were determined as the center of the interplays during the entire crystallographic phenomena.

(Received February 14, 2017; accepted April 5, 2018)

Keywords: Absorption spectroscopy, Electronic structure, Crystal Properties, Oxides

1. Introduction

Rare-Earth orthoborates have a high potential in recent technological applications due to their desirable electrical, electronic and magnetic properties. The interesting phenomena occurring between *3d* Transition Metals (TM) and *4f* Rare-Earths (RE) have been reported in various studies and they cause a huge demand to perform investigations on 3*d*-4*f* originated interactions [1-3]. Narrow band structure and rich quantum symmetries of RE *4f* levels, keep them in the center of the molecular reactions. However, in such materials, the main role is assigned to 3*d* elements due to possessing convenient quantum symmetries both for the light and heavy atoms. So, they are treated as the most active elements in building up large molecular bands via overlapped *p-d-f* hybridization. In other words, the 3*d* levels of TM atoms act as a link between the heavy RE's 4*f* electrons with light atoms (i.e. O, S, B, etc.). Besides, *d*-levels mostly presented in the molecular bands via hybridization that supports the excited electrons' transition to broad hybridized levels against quantum selection rules. Like RE elements, transition metals and their oxides are also leading materials for current and future technologies with their desired chemical, crystallographic, magnetic and electronic transport properties. Both TM's and RE's are members of the Strongly Correlated Electron Systems (SCES) family due to their highly active, partly filled *d* and *f* shells which can emerge strong electronic correlations with the outer shell electrons of their neighbor atoms.

In this study, influences of Sm (Samarium) substitution on the electronic and crystal properties of the Ferric Borate ($FeBO_3$) structure were investigated. $(Sm_xFe_{1-x})BO_3$ structure is the general formula for this study, where Boron was also considered as a key agent. Boron, in the structure, plays an important role because of possessing higher affinity and has high electron deficiency with highly vacant *p*-orbital. Besides, the thermal stability makes borates an important tool for high temperature devices and nonlinear optical materials [4].

The parent oxide $FeBO_3$ is a member of the transition metal boron oxides with $M^{3+}BO_3$ general formula and have been studied intensively. The group has been reported to form in trigonal geometry with rhombohedral symmetry and a space group of "*R-3c*" (D_{3d}^6) [5, 6]. It shows weak antiferromagnetic (AFM) ordering with a Neél temperature of 348 K (75 ^oC) [7, 8]. Additionally, in previous studies on ABO_3 type materials, where A is a rare-earth element and B is a transition metal, TM's were reported as the main actor determining the catalytic activity for oxidation [9, 10].

As one of the product of the studied materials, $(RE)BO_3$ group is also popular due to their abilities showing nonlinear optical properties [11]. Also, nanoscale samples of the $(RE)BO_3$ group are of interest due to showing biological fluorescence labels or high resolution abilities as phosphor components in plasma display panels [12]. Rare-Earth orthoferrites were reported as rich materials to study the relations in the electronic and magnetic interactions between TM's and RE's where Rare-Earth's were treated as the key elements [13-15]. $SmFeO_3$ crystal was first studied by Marezio et al. in 1970 [16]. In the study, $SmFeO_3$ crystal structure was reported as similar to the distorted perovskite $CaTiO_3$. Besides, in another study on Rare-Earth Orthoferrites, Maslen et al. reported that the interactions between Sm-Fe atoms have major influence on the magnetic ordering and spin configurations of the Fe atoms [17]. Moreover, responses

of Ni substitution into Fe coordinations were studied by Bashir et al. in 2010 for the SmFeO3 In this paper, the electronic, magnetic and crystal structure properties of the SmFeO3 material with a canted AFM ordering in the structure was reported [18]. An additional study on Ho substitution was reported by Baharthi et al. (2011) [19]. However, the general formula of $Sm_xFe_{1-x}BO_3$ has not been subject to any study, yet.

2. Experimental

The samples were prepared at the Advanced Materials Research (MEITAM) laboratories of Mersin University (Mersin, Turkey) and synthesized from the stoichiometric mixtures of Sm_2O_3, Fe_2O_3 and B_2O_3 powder compounds as starting materials with high purity (>99.99%) by the solid state reaction method with the general formula of $Sm_xFe_{1-x}BO_3$, for the values of x as 0, 0.2, 0.5, 0.8 and 1. Mixed powders were milled for 30 minutes and calcined in air at 823 K (550 ^oC) for 4 h. After the first annealing process, mixed powders were milled again for 30 minutes and annealed in air at 1223 K (950 ^oC) for 48 h. To identify the characteristics of the crystal structures in the samples and to support related crystal structure analysis, XRD patterns were taken at MEITAM laboratories with Rigaku Smartlab model. Besides, to determine the electrical characteristics of the samples, electrical resistivity measurements were performed with the four probe technique at room temperatures (RT).

Magnetic properties of Sm substituted ferric borate samples were tested with PPMS system with Field Cooled measurements under 1kOe magnetic field and samples were determined to have weak AFM ordering at the room temperatures like in the study by Troyan et al. for the $FeBO_3$ oxide [20].

For the investigation of the details of the crystal structure formations in the samples with the Sm substitution, the X-ray Absorption Near Edge Spectroscopy (XANES) measurements were performed. XANES technique is one the best tools for providing rich data collection for detailed electronic and crystal structure analysis of the materials. XANES region on the absorption spectra lies between an energy range of approximately 30-50 eV below and 70~100 eV above the absorption edge of elements. XANES data can provide information about the bonding with the neighboring atoms, electronic structure of the interested atom in the materials and support the determination of the local atomic arrangements in the materials [21-23].

For the study of electronic properties of the samples in soft x-ray region, XANES measurements were performed at MAX-Lab synchrotron radiation facility of Lund University in Lund (Sweden). Fe $L_{3,2}$-edge and O K-edge XANES data were collected at Beamline I1011 on MAX-Lab in TEY (Total Electron Yield) mode. The beamline I1011 is located on the ring MAX-II, uses an elliptically polarizing undulator and provides soft x-ray with a variable polarization state [24]. XANES measurements were performed at room temperature and under ultra high vacuum (UHV) (~10^{-10} Torr) conditions. Additionally, XANES data in the hard x-ray region were collected from the Sm L_2 -edge and Fe K-edge of the $Sm_xFe_{1-x}BO_3$ samples at Beamline-BL8:XAS of Siam Photon (SLRI) Synchrotron Radiation facility in Nakhon Ratschasima, Thailand [25, 26]. The beamline operates for X-ray Absorption Spectroscopy, serves a high flux light from a bending magnet and has an energy range of 1.25 keV to 10 keV. The measurements were performed at room temperature in transmission mode.

3. Results and discussion

Electrical properties of the samples were measured by the collected electrical resistivity data with four-probe technique at the room temperatures and the results for $Sm_xFe_{1-x}BO_3$ samples are given in Figure 1. On the right column of figure 1, calculated average crystallite sizes of the samples are also given for comparison. Several studies have been published reporting the relation between the electrical conductivity properties of the samples with their crystal morphology [27]. In this manner, average crystallite sizes were calculated according to the Scherrers' formula via taken XRD patterns (given in figure 2) of the samples [28]. According to the figure, an agreement observed with the resistivity and the average crystallite sizes of the figure, except sample for x=0.2. Resistivity of the samples were measured between a range of 2.0~7.0 10^6 ohm.cm. Four probe measurement results revealed that all samples are members of weak semiconductors class. Among the samples, $SmBO_3$ (x=1.0) was determined to have the highest electrical resistivity among the samples. Lower resistivity of the Sm substituted sample than $SmBO_3$ sample highlights the effect of interacting "Sm-Fe" neighbors on the whole electronic processes leading to higher conductivity in the sample. In the electrical resistivity responses of the iron containing samples, a slight increase for x=0.5 substitution observed, while resistivity for the sample x=0.8 was measured as the lowest among studied samples. According to the given crystal structure results in table 1, the figure confirms the change in the crystalline sizes and has a direct influence on the resistivity of the materials. Besides, the change in the measured electrical resistivity of the samples revealed phase transitions in the crystals by the rare earth substitution. Interplays between neighboring atoms in the sample that cause such and electrical resistivity differences would be more clear with the further crystal and electronic studies.

Table 1. The XRD pattern results of Sm doped $FeBO_3$ samples.

Substitution ($Sm_xFe_{1-x}BO_3$)	Crystal	α	β	γ	a	b	c	Geometry	SG	%
X=0	$FeBO_3$	90	90	90	5.036	5.306	13.751	Trigonal	R-3c:H	100
X=0.2	$FeBO_3$	90	90	90	5.028	5.028	13.710	Trigonal	R-3c:H	80
	$SmBO_3$	107.63	107.42	93.33	6.468	6.500	6.245	Triclinic	P1	20
X=0.5	$FeBO_3$	90	90	90	5.412	5.412	13.424	Trigonal	R-3c:H	49
	$SmBO_3$	133.96	91.39	88.11	5.703	9.043	6.725	Triclinic	P1	51
X=0.8	$SmBO_3$	107.22	106.96	93.62	6.479	6.489	6.272	Triclinic	P1	80.5
	$FeBO_3$	90	90	90	4.617	4.617	14.663	Trigonal	R-3c:H	19.5
X=1.0	$SmBO_3$	107.23	107.00	93.549	6.476	6.491	6.268	Triclinic	P1	100

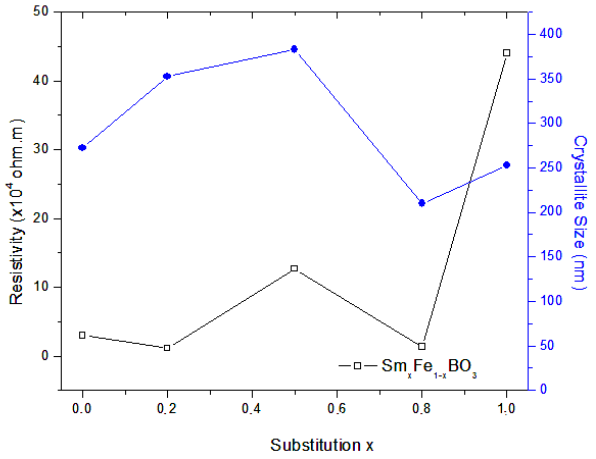

Fig. 1. Measured electrical resistivity and estimated crystallite sizes of Sm-doped $FeBO_3$ samples

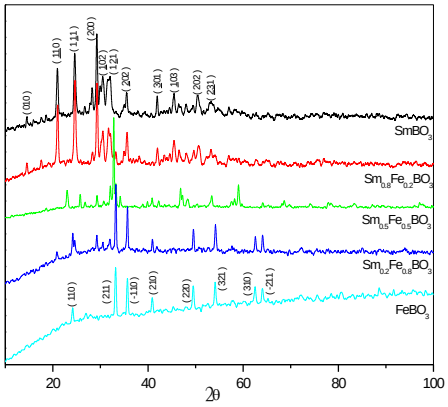

Fig. 2. Compared XRD patterns of $Sm_xFe_{1-x}BO_3$ samples

To reveal the background information of the electrical properties in the samples, we need to understand the structural (crystal&electronic) properties in the samples that may provide us useful tools for more detailed analysis. For this purpose, XRD patterns of the samples were also taken as given in figure 2, related crystal structure analysis were done by the MAUD software [26] and given in Table 1. In Fig. 2, as a result of powder form of the samples, all patterns show somehow noisy background structure. Also, noise-like multiplet pattern for the samples x=0.8 and 1.0 reflects polymorphism in the structures. The diffraction pattern of the sample for x=0.0 (i.e. Pure $FeBO_3$) has multiplet peak feature with lower noise than other samples, adressesing one type crystalline structure formation in the material. Along with the crystal analysis, the sample for x=0.0 was determined to have single crystal structure "$FeBO_3$" with Rhombohedral geometry and "*R-3c:H*" space group symmetry. Determined parameters for the parent sample $FeBO_3$ and other samples are given in table 1.

According to the XRD patterns of the Sm substitutions, the samples for both x=0.0 and 0.2, the patterns showed similar reflection peaks with the pure $FeBO_3$ sample. In such a case, we can conclude that, the substituted samarium atoms highlight their positioning in Fe coordinations. However, if a heavy fermion atom sit in a *3d* row metals location there should be differences on the reflection peak locations in the XRD patterns. The pattern for the sample x=0.2 has so weak changes or shifts that is difficult to realize but the peak shifts and intensity changes for the sample x=0.5 is visible. Pattern for the 0.2 value of x, the Sm locations only give so weak reflections about 30 degrees (2θ) highlighting Sm atoms tend to form different crystal structure at isolated regions in the bulk. However, the same reflection peak became stronger for the sample "x=0.5" and the rest have different reflection peaks than the samples for x=0.0 and 0.2. According to the crystal structure analysis, the substituted "Sm" atoms prefer to keep them as isolated regions and formed in triclinic $SmBO_3$ structure, while iron atoms remained in its stable geometry $FeBO_3$. The slight change in peak formation

became obvious in the sample for x=0.5 due to the heavy atom with more atomic concentration than Fe and sitting away from the light Fe atoms positions. The change in the atomic concentrations also cause changes in lattice parameters of the samples x=0.2 and 0.5 which were determined to form in the same crystal structure both for Fe and Sm. Iron and samarium atoms bond with different BO_3 ligands and boron became the main star of the interplays by controlling them via strongly bonding with oxygens.

The XRD pattern results for the sample x=0.8 has noisy and multiplet peak structure that highlights the formation of a polycrystalline material with a lower symmetry in the bulk. In the sample for x=0.8, triclinic $SmBO_3$ structure was determined to form dominantly in the bulk. Rest of the crystal was determined to form in iron originated parent oxide $FeBO_3$ (19.5%). The crystal structure formations highlights that heavy fermion samarium atom tends to form isolated domains and did not intend to have any molecular interplay to construct a molecular band via an overlapping. The triclinic $SmBO_3$ structure has determined to build its environment with the space group symmetry of "*P1*". Lower site symmetries of the crystal geometries supports the noisy character of the XRD patterns. However, the low site symmetry in the crystal geometries seem to support the unusual electrical properties that decreases the resistivity (as seen in Fig. 1) by providing longer distances that electrons can hop.

Atomic interactions yielding different crystal structure formation in the samples is related with their electronic properties and XANES spectroscopy can provide fruitful information about the bonding mechanisms along with the electronic structure. For the 3*d* transition metals, K and L-edges are so sensitive to the interactions with the neighboring atoms and the chemical states of the atoms where 1*s* and 2*p* electrons transition to the empty levels over the Fermi level as a final state takes place, respectively. 3*d* level of TM's is located just below the Fermi level and give clues about the bonding properties of the source atoms.

XANES region can be studied into two regimes; the pre-edge and the post-edge. The pre-edge structure lies just below the main absorption edges and highlights the forbidden transitions, crystal disorders, asymmetries etc., in other words it gives a picture of disorders in the crystal or electronic structures. The post-edge part is just located beyond the main edge and also provides information about the interactions between the closest neighboring atoms. In Fig. 3, Fe K-edge XANES spectra for the sample $Sm_{0.5}Fe_{0.5}BO_3$ (x=0.5) is given. The sample for x=0.5 was picked up to visualize the electronic properties when the main geometries share the same amount and due to having highest resistivity among substituted samples. Therefore, the sample can give us a chance to see the electronic mechanisms on a balanced ratios of Sm and Fe locations. The K-edge absorption spectra of iron in the sample begin to rise at 7109 eV and have a maximum at 7130.6 eV. On the spectra, no remarkable pre-edge structure observed, which means no forbidden transition or asymmetric bonding occurred in the samples. For 1*s* electrons' transition to 3*d* level as a final state is forbidden according to quantum selection rules. So, possible route for excited electrons' are the *4p* levels above the Fermi level as a final state. Pre-edge structure works like an agent indicating the asymmetry in a crystal or occurred forbidden transitions. This result also confirms the geometries formed without asymmetries in the sample; i.e., orthorhombic and trigonal.

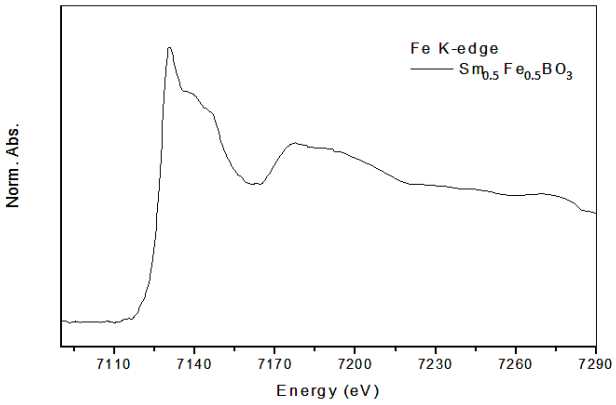

Fig. 3. Fe K-edge XANES spectra of the sample for x=0.5, i.e., $Sm_{0.5}Fe_{0.5}BO_3$

The main absorption edge has a sharp intensity which is related with the amount of the unoccupied states at the valence levels. Broad main edge feature reflects available unoccupied states on the *4p* levels. Absorption spectra due to transitions to the *4p* level have three peaks on the main edge because of the crystal field effect for 4(p_x, p_y and p_z). First "strong" peak is a low energy level on the molecular band (t_{2g}) where electrons from 1s level sits as a final state in Fe^{4+} ions. Beyond this peak, two bump-like peaks have appeared as high (e_g) energy levels on the molecular band from the Fe^{3+} ions in the $FeBO_3$ structure.

In Fig. 4, the Fe $L_{3,2}$-edge spectra of the sample ($Sm_{0.5}Fe_{0.5}BO_3$) is also given. The L-edge was selected due to the higher sensitivity for the valence levels (strong coupling with valence electrons) and possibility to provide more elaborate data both for electronic properties. Because $L_{3,2}$-edge transitions are result of *2p* electrons transitions to unoccupied states below the Fermi level, i.e., *3d*. So this spectra can give us precious tools to probe the *3d* level of the atoms in the samples. The L_3-edge begin to rise at 704.7 eV and the main edge feature consist of two peaks with a lower intensity at 707.16 eV and a peak with higher intensity at 708.45 eV. As mentioned above, the pre-edge feature on an absorption edge may appear below the main edge as a result of forbidden electronic transitions ($\Delta l \pm 1$) or asymmetries in the crystal structure. The L_3-edge absorption spectra is due to 2*p* electrons' transition to 3*d* levels and obeys dipole selection rules. Besides, high symmetry in the crystal geometries for x=0.5 should support the "no pre-edge" feature. The peak with lower absorption intensity at 707.16 eV correspond to $2p_{3/2}$ electrons transition to low energy levels t_{2g} in Fe^{4+} ions. The peak with higher intensity beyond the pre-edge at 708.45 eV is due the transition route of $2p_{3/2}$ electrons to

3*d* levels and addresses Fe^{3+} ions in the bulk. L_2-edge absorption spectra of the sample has also a two peaks. At 717.4 eV, the L_2-edge absorption spectra begin to rise and have two maxima at 720 and 721.7 eV like the L_3 edge spectra, respectively.

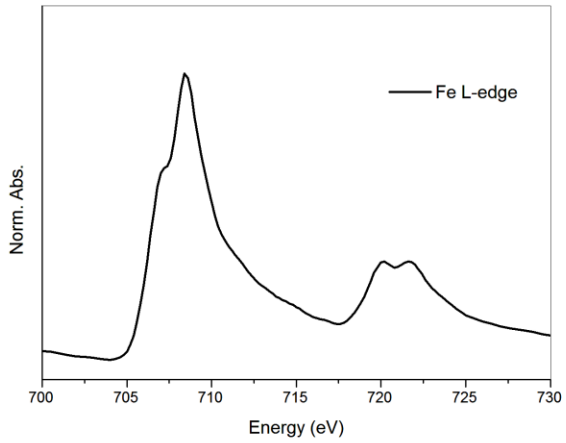

Fig. 4. Fe $L_{3,2}$-edge spectra of the sample $Sm_{0.5}Fe_{0.5}BO_3$

In Fig. 5, Sm L_2-edge absorption spectra of the sample $Sm_{0.5}Fe_{0.5}BO_3$ is given to investigate the traces of Sm-Fe interplay. The spectra begin to rise at 7300 eV and has a smooth main edge with a maximum at 7319.12 eV which corresponds to the 2*p* electrons transition to the 5*d* levels of Samarium. Actually, 4*f* levels of Sm atoms are unoccupied and offer convenient holes as a final state for excited electrons, however, due to the quantum selection rules *p* electrons' transition to 4*f* levels is forbidden. The spectra of Sm in the figure has a smooth absorption spectra, without any bump or a weak edge at the pre-edge side, confirming no forbidden transition ($2p \rightarrow 4f$) exists. In case of any interaction between Fe *3d* and Sm *4f* levels, a hybrid level may created and this level should attract excited electrons to the empty states. If so, there should be a low energy level on the molecular band with a characteristics of *f*-like *d*-level as a final state for some low energy excited electrons. Such a process can appear below the main edge as small peak seperately and named as pre-edge. In such a complicated structure, oxygen atoms pretends like a bridge between Sm and Fe atoms. In other words, O 2*p* levels are the only way for 4*f* and 3*d* levels to interact with eachother, but weakly via hybridization. Smooth spectra of Sm (in Fig. 5) and Fe (in Fig. 4), without pre-edge, confirms oxygen bonding with Sm via 5*d* band while with iron bonded via 3*d* levels.

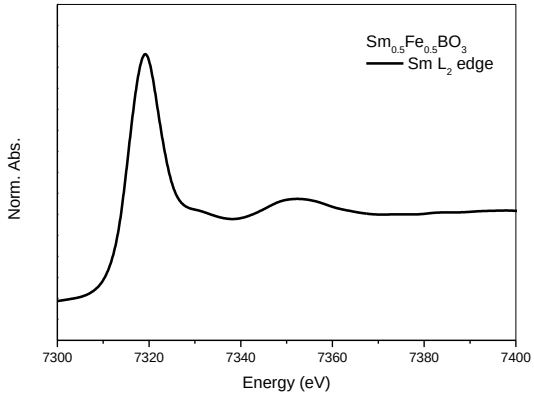

Fig. 5. Sm L_2-edge XANES spectra of the sample $Sm_{0.5}Fe_{0.5}BO_3$

In Fig. 6, Fe $L_{3,2}$-edge spectra of the samples $FeBO_3$, $Sm_{0.2}Fe_{0.8}BO_3$ (x=0.2) and $Sm_{0.5}Fe_{0.5}BO_3$ (x=0.5) are given in comparison. $FeBO_3$ structure with narrower bandwidths stands out in L-edge absorption spectra from the Sm-doped samples. That was appeared due to the narrower molecular bands formed by O2*p*-Fe3*d* hybridized levels. In $FeBO_3$, the Fe 3*d*-O 2*p* hybridized levels have weaker and lower intensity than others, where the electronic transitions only have a route from Fe 2*p* levels to unoccupied 3*d* levels as a final state, due to the influence of boron on the oxygen atoms.. In other words, presence of B atoms weaken the strong overlapping between Fe 3*d*-O 2*p* due to higher electronegativity of boron. Boron sits in the center of the ligand linked to oxygen atoms and isolate themselves from metals (Sm, Fe). Only oxygen is the element which sits in the cross roads of molecular interactions.

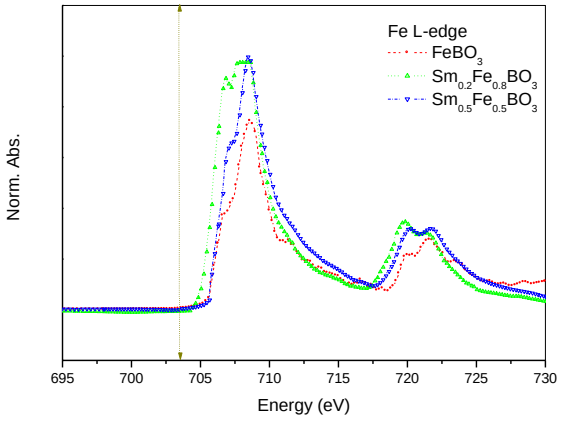

Fig. 6. The compared Fe $L_{3,2}$-edge spectra of the samples $FeBO_3$, $Sm_{0.2}Fe_{0.8}BO_3$ and $Sm_{0.5}Fe_{0.5}BO_3$

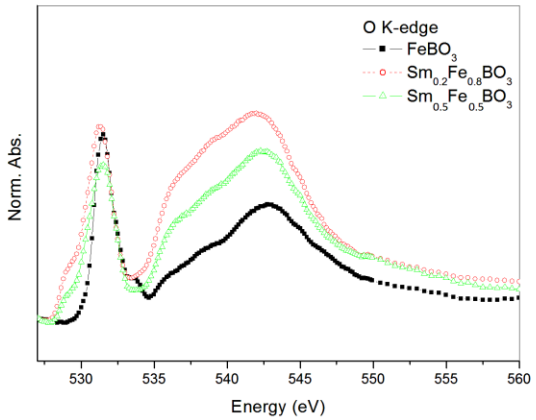

Fig. 7. Compared Oxygen K-edge spectra of $FeBO_3$, $Sm_{0.2}Fe_{0.8}BO_3$ and $Sm_{0.5}Fe_{0.5}BO_3$ samples

To analyze this interplay better, O K-edge XANES spectra would be the best choice to observe the bonding interactions in detail, as given in Fig. 7. Main absorption edge of oxygen atoms corresponds to 1*s* core electron transitions to 2*p* energy levels. The O K-edge spectra of the samples consist of two parts; a sharp pre-edge and a large main edge. The pre-edge in $FeBO_3$ sample begin to rise at 528 eV and have maximum at 531.4 eV as the pre-edge feature due to O2*p*-Fe3*d* hybridization. Also, at 533.7 eV, beyond the main pre-edge peak, a shoulder like peak at higher energy level observed due to strong overlapping between O 2*p* and Fe 3*d* levels in the $FeBO_3$ sample. The intensive peak of the pre-edge structure of the samples confirms high amount of available states on the hybridized *3d-5d* levels of Fe and Sm. O K-edge spectra of the samples for x=0.2 and 0.5 have broader pre-edge peaks than $FeBO_3$ due to Sm *5d* contribution and a weak pre-edge feature appeared at 529 eV. This new feature appears as a result of hybridization between Sm 5*d*-O 2*p*. The contribution of the Sm *5d* level to the bonding provides larger pre-edge structure emphasizing strongly overlapped molecular bands with higher symmetries. The *5d* contribution is more clear with x=0.2 sample who has larger and more intense pre-edge peak than others. Main absorption edge in the $FeBO_3$ structure has a maximum at 542.9 eV. However, for the samples x=0.2 and 0.5 have slight energy shifts to the lower energy side, due to *5d* extra rich quantum symmetry of Sm as 0.7 eV and 0.3 eV, respectively.

4. Conclusion

In this study, the crystal and electronic properties of Sm doped $FeBO_3$ samples were investigated by x-ray based spectroscopic techniques; XRD pattern analysis and XANES. Phase transitions and polycrystalline characteristics in the crystal structures were determined due to the increasing Sm substitutions. Besides, the influence of Boron on the properties of the crystals were confirmed to act on the mechanisms and yield polycrystalline structures influencing the electric and electronic properties. In the early stages of the substitutions, the crystal structure preserved its stable form even Sm doping and $FeBO_3$ crystal structures were observed with the increasing doping rate of Sm atoms. In the Sm substituted samples, Sm atoms were determined to have a tendency to form in triclinic "P1" symmetries.

According to the sample analysis, Fe atoms were determined to have a strong influence on the entire interactions in the samples. Fe atoms build up links with other members via oxygen bonding. Besides, oxygen atoms were determined as the only meeting point for all elements. But, boron has determined as the main role player in all molecular interplays by bonding with oxygen atom strongly and form BO_3 ligands. Due to strong influence of boron on the oxygen atoms, iron and samarium atoms conditioned to bond with oxygen atoms via BO_3 ligands and possessed limited crystal structure oppurtunities during bonding to form the crystal.

Acknowledgement

The authors would like to thank to Dr. Gunnar Ohrwall from MAX-lab. Beamline I1011 in Lund, Sweden. Also, we would like to thank to Dr. Wantana Klyusubun and her staff from SLRI (Siam Photon) both for their technical support and great hospitality.

This study is supported financially by "BAP-TTEF EEEME (OMÖ) 2012-7" project of Mersin University (Mersin, Turkiye).

Additionally, the research leading to these results has received funding from the European Community's Seventh Framework Program (FP7/2007-2013) CALIPSO under grant agreement no 312284.

References

[1] C. Ruihua, C. N. Borca, P. A. Dowbena, S. Stadler, Y. U. Idzerda, Applied Physics Letters **78**(4), 521 (2001).
[2] H. S. Nabi, R.Pentcheva, Physical Review B **83**, 214424 (2011).
[3] E.A. Moore, Physical Review B **76**, 195107 (2007) .
[4] Y.W. Liu, X.F. Rui, Y.Y. Fu, Y.W. Han Zhang, J. of Metastable and Nanocrystalline Materials **23**, 243 (2005).
[5] I. Bernal, C. W.Struck, J. G.White, Acta Crsyt. **16**, 849 (1963).
[6] H. Schmid, Acta Crsyt. **17**, 1080 (1964).
[7] J. C. Joubert, T. Shirk, W. B. White, R. Roy, Mater. Res. Bull. **3**, 671(1968).
[8] N. V. Kazak, A. M. Potselvyko, S. G. Ovchinnikov, A. S. Alexandrovski, V. A. Chernov, V. V. Rudenko, Physica B **378-380**, 327 (2006).
[9] L. G. Jejuca, J. L. Fierro, J. M. D. Tascon, Adv. Catal. **36**, 237 (1989).
[10] M. Misono, Stud. Surf. Sci. Catal. **54**, 13 (1990).
[11] P. Becker, Advanced Materials **10**, 979 (1998).
[12] Z. Li, J. Zeng, Y. Li, Small **3**, 438 (2007).

[13] M. W. Lufoso, P. M.Woodward, Acta Cryst. **B57**, 725 (2001).
[14] R. L. White, J. App. Phys. **40**, 1061 (1969).
[15] R. M. Bozarin, D. Williamsh, E.Walsh, Phys. Rev. **103**, 572 (1956).
[16] M. Marezio, J.P. Remeika, P.D. Dernier, Acta Cryst. B **26**, 2022 (2008).
[17] E. N. Maslen, V. A. Sterltsoy, N. Ishizawa, Acta Cryst. **B 52**, 406 (1996).
[18] A. Bashir, M. Ikram, R. Kumar, P. N. Lisboa-Filho, P. Thakur, Materials Science and Engineering B **172**, 242 (2010).
[19] K. K. Baharthi, G. Markandeyulu, C. V. Ramana, J. Phys. Chem C **115**, 554 (2011).
[20] I. A. Troyan, A. G. Gavrilyuk, S. G. Ovchinnikov, I. S. Lyubutin, N. V. Kazak, JETP Letters **94**(10), 748 (2011) .
[21] A. L. Ankudinov, B. Ravel, J. J. Rehr, S. D. Conradson, Phys. Rev. B **56**, R1712 (1997).
[22] B. Ravel, Journal of Synchrotron Radiation **8**(2), 314 (2001).
[23] B. Ravel, M. Newville, Journal of Synchrotron Radiation **12**(4), 537 (2005).
[24] I. A. Kowalik, G. Öhrwall, B. N. Jensen, R. Sankari, E. Wallen, U. Johansson, O. Karis, D. Arvanitis, J. of Physics: Conference Series **211**, 012030 (2010) .
[25] W. Klysubun et al., Nuclear Instruments and Methods in Physics Research A **582**, 87W (2007).
[26] W. Klysubun et al., AIP Conference Proceedings **879**, 860 (2006).
[27] A. Tschöpe, Solid State Ionics **139**(3–4), 267 (2001).
[28] H. O. Abd-Alkader, N.M. Dearz, Int. J. Electrochem. Sci. **8**, 8614 (2013).
[29] R. Wolfe, R. D. Pierce, M. Eibschütz, J. W. Nielsen, Solid State Communications **7**(13), 949 (1969).

*Corresponding author: ozkendir@gmail.com